

# Hierarchical Diffusion Motion Planning with Task-Conditioned Uncertainty-Aware Priors

Amelie Minji Kim, Anqi Wu<sup>†</sup>, and Ye Zhao<sup>†</sup>

**Abstract**—We propose a novel hierarchical diffusion planner that embeds task and motion structure directly into the noise model. Unlike standard diffusion-based planners that rely on zero-mean, isotropic Gaussian corruption, we introduce task-conditioned structured Gaussians whose means and covariances are derived from Gaussian Process Motion Planning (GPMP), explicitly encoding trajectory smoothness and task semantics in the prior. We first generalize the standard diffusion process to biased, non-isotropic corruption with closed-form forward and posterior expressions. Building on this formulation, our hierarchical design separates prior instantiation from trajectory denoising. At the upper level, the model predicts sparse, task-centric key states and their associated timings, which instantiate a structured Gaussian prior (mean and covariance). At the lower level, the full trajectory is denoised under this fixed prior, treating the upper-level outputs as noisy observations. Experiments on Maze2D goal-reaching and KUKA block stacking show consistently higher success rates and smoother trajectories than isotropic baselines, achieving dataset-level smoothness substantially earlier during training. Ablation studies further show that explicitly structuring the corruption process provides benefits beyond neural conditioning the denoising network alone. Overall, our approach concentrates the prior’s probability mass near feasible and semantically meaningful trajectories. Our project page is available at <https://hta-diffusion.github.io>.

## I. INTRODUCTION

Diffusion models have garnered increasing attention in robotic motion planning and shown strong flexibility across tasks [1], [2], [3], [4], [5]. However, most existing approaches adopt a default corruption process using zero-mean, isotropic Gaussian noise, overlooking the inherent structure of robotic trajectories. In contrast to image or text data, robotic motion possesses intrinsic properties such as temporal smoothness (e.g., consistent evolution across time steps for dynamic feasibility) and can also be shaped by structured external information, such as task-imposed conditions (e.g., start and goal states or phase-specific constraints). These structured sources of information provide inductive biases that diffusion models can exploit, most commonly through conditioning or guidance [3], [6], [7], [8], [1].

In this work, we propose to encode such structure in the form of a task-aware noise model. This design enables our diffusion planner to respect smoothness and constraint satisfaction by construction. We realize this idea with a two-level hierarchical diffusion framework. The upper-level

planner produces sparse, task-centric key states (or key constraints). We treat these key states as soft observations with explicit uncertainty, allowing imperfect predictions to guide sampling without hard constraints or rejection. The lower-level diffusion then generates the full trajectory under a task-conditioned Gaussian, obtained by conditioning a linear time-varying Gaussian process (LTV-GP) motion prior on the key states, inspired by Gaussian process motion planning (GPMP) [9]. This yields a non-isotropic, temporally correlated noise model whose mean and covariance encourage smooth dynamics between key states, while the key states act as anchors that prevent global oversmoothing and allow the trajectory to adapt at sharp turns or task-phase changes. Accordingly, this framework produces temporally consistent and constraint-aware plans.

Previous diffusion works typically keep the corruption isotropic and inject structural constraints through conditioning or guidance during inference [8], [1], [2]. For instance, conditioning has been used to incorporate visual context from observations or to inject goal information [3], [6]. Guidance mechanisms and auxiliary objectives incorporate dynamics, task rewards, or safety specifications into the generative process [10], [11]. In addition to conditioning and guidance, task-centric representations have been leveraged to encode constraints, for example object-centric demonstrations [12] or SE(3)-based cost fields that couple grasp and motion optimization [13]. Projection-based methods have also been explored, where diffusion samples are mapped into feasible sets such as dynamically admissible trajectories [14] or collision-free multi-robot paths [15]. Beyond these categories, diffusion models have also been integrated with model-based plan [16] or with neural dynamics models [17].

Structured corruptions during training have been explored primarily outside robotics. Examples include non-Gaussian but zero-mean choices [18], per-pixel variance schedules without temporal or robotics priors [19], and non-isotropic formulations that capture joint dependencies in human pose but still assume zero-mean noise and omit temporal correlations along the horizon, limiting their use for trajectory state conditioning [20]. Mixture priors have also been proposed for multimodality and controllability, where Gaussian mixture parameters may be predefined through clustering [21] or heuristic structure [22], learned end-to-end to adaptively cover target support [23], or dynamically adjusted during inference by solver-based approaches [24]. In robotics, structured corruptions remain rare, with only a few recent efforts—for example, integrating coarse trajectory predictions

A. M. Kim and Y. Zhao are with the Institute for Robotics and Intelligent Machines (IRIM), Georgia Institute of Technology, Atlanta, GA 30308, USA. [mkim955@gatech.edu](mailto:mkim955@gatech.edu); [ye.zhao@me.gatech.edu](mailto:ye.zhao@me.gatech.edu)

A. Wu is with the School of Computational Science and Engineering, Georgia Institute of Technology, Atlanta, GA 30308, USA. [anqiwu@gatech.edu](mailto:anqiwu@gatech.edu)

<sup>†</sup> Co-senior authorship

so that diffusion acts as a refiner [25], introducing temporally correlated noise such as colored Gaussian perturbations [26], or employing diffusion bridges that initiate denoising from informative prior actions in navigation tasks [27]. While these studies highlight the benefits of structured corruptions for distributional expressiveness, they do not leverage structured priors to encode task conditions and temporal smoothness simultaneously. In contrast, our design directly biases the generative process toward trajectories that are both dynamically consistent and task-aware, rather than only improving multimodality.

Hierarchical diffusion has been used to separate coarse-level decisions from finer-level motion, for example: subgoal generation followed by refinement [28], cascaded global and local prediction with online repair [29], progressive coarse-to-fine refinement processes that achieve real-time planning frequencies [30], contact-guided manipulation policies that decompose high-level contact planning from low-level trajectory generation [31], kinematics-aware frameworks with high-level end-effector prediction and low-level joint generation [32], and diffusion–flow hybrids that pair high-level diffusion with low-level rectified flow [33]. A common pattern feeds high-level outputs to the low level as conditioning, while low-level corruption remains isotropic. This leaves the forward process and loss unchanged, while low-level corruption remains isotropic. Our hierarchy instead reparameterizes the low-level prior by conditioning a GP on upper-level key states. This yields a trajectory posterior whose mean interpolates the key states and whose covariance couples time steps, so reverse diffusion operates in a Mahalanobis geometry that restricts sampling to trajectories consistent between key states while modeling key-state uncertainty. This improves feasibility without post hoc constraints or rejection.

We evaluate on Maze2D goal reaching and KUKA block stacking from the Diffuser benchmarks [2]. We compare (i) a single-layer diffuser with isotropic noise, (ii) a hierarchical diffuser with conditioning only, (iii) a diffuser with cost guidance at inference, and (iv) our full hierarchical model with a structured, key-state–conditioned prior. Across tasks, our model outperforms all the baselines, indicating that embedding structure in the generative noise yields consistent gains in task success over just conditioning or guidance.

Our contributions are summarized as follows:

- A two-level hierarchical diffusion planner where the upper-level planner infers sparse, task-centric key states and the lower-level planner denoises under a GPMP-based motion prior conditioned on them. Key states are treated as soft observations with explicit uncertainty, encoding smoothness while encouraging satisfaction of task constraints without imposing hard constraints.
- A diffusion formulation with *task-conditioned* non-isotropic Gaussian corruption, obtained by conditioning a GPMP-based prior on key states, with closed-form forward marginals and posteriors for variational training. This yields a Mahalanobis loss that generalizes MSE while preserving the standard DDPM pipeline.

- Experiments on Maze2D goal reaching and KUKA block stacking show higher success and better constraint satisfaction than isotropic and conditioning-only baselines, validating that reparameterizing the low-level prior reshapes the diffusion landscape and concentrates samples around key-state–consistent trajectories.

## II. PRELIMINARY

### A. DDPM for motion planning

Let a robot trajectory be a stacked sequence of states  $\tau = [x_1; \dots; x_H] \in \mathbb{R}^{H \cdot d}$ , where  $x_t \in \mathbb{R}^d$  is the robot state at time step  $t$  and  $H$  is the planning horizon. We denote by  $\tau^i$  the trajectory after  $i$  forward diffusion steps.

Diffusion models learn to denoise trajectories that are gradually corrupted by Gaussian noise. Under the standard DDPM corruption [34], the forward process is

$$\tau^i = \sqrt{\alpha_i} \tau^{i-1} + \sqrt{1 - \alpha_i} \varepsilon, \quad \varepsilon \sim \mathcal{N}(0, I), \quad (1)$$

where  $\alpha_i := 1 - \beta_i$  for  $i = 1, \dots, N$ ,  $\{\beta_i\}_{i=1}^N \subset (0, 1)$  is a scalar variance schedule, and  $N$  is the total number of diffusion steps. Let  $\bar{\alpha}_i := \prod_{k=1}^i \alpha_k$ . Then the closed-form marginal is

$$\tau^i | \tau^0 \sim \mathcal{N}(\sqrt{\bar{\alpha}_i} \tau^0, (1 - \bar{\alpha}_i)I).$$

The one-step reverse posterior is also Gaussian,

$$q(\tau^{i-1} | \tau^i, \tau^0) = \mathcal{N}(\tau^{i-1}; \hat{\mu}_i(\tau^i, \tau^0), \hat{\beta}_i I), \quad (2)$$

where  $\hat{\mu}_i$  and  $\hat{\beta}_i$  are the posterior mean and variance coefficient at the  $i^{\text{th}}$  diffusion step (closed forms omitted for simplicity).

A denoising network  $\mu_\theta(\tau^i, i, \text{cond})$  is trained to predict the posterior mean with the objective

$$\mathcal{L}(\theta) = \mathbb{E}_q \left[ \left\| \hat{\mu}_i - \mu_\theta(\tau^i, i, \text{cond}) \right\|_2^2 \right], \quad (3)$$

where `cond` may include initial and goal states, maps, waypoints, or other task variables. At test time, sampling runs the reverse Markov chain starting from  $\tau^N \sim \mathcal{N}(0, I)$ .

In Sec. III, we generalize (1) by biasing the mean and allowing a *non-isotropic* covariance in the corruption process. The standard DDPM is recovered as  $\mu = 0$  and  $\mathcal{K} = I$ .

### B. Gaussian Process Motion Planning

Gaussian Process Motion Planning (GPMP) models a continuous time trajectory as a Gaussian process (GP), i.e.,

$$x(t) \sim \mathcal{GP}(\tilde{\xi}(t), \tilde{\mathcal{K}}(t, t')), \quad (4)$$

whose mean and kernel are induced by a linear time varying (LTV) dynamics prior [9]. Consider the stochastic LTV model  $\dot{x}(t) = A(t)x(t) + u(t) + w(t)$  where  $u(t)$  is control input and  $w(t)$  is zero mean white noise with spectral density  $Q_C \succeq 0$ . Let the initial mean and covariance at time  $t_0$  be  $\xi_0$  and  $\mathcal{K}_0$ , and let  $\Phi(t, s)$  denote the state transition matrix of  $A(\cdot)$ . Then the GP has mean  $\tilde{\xi}(t) = \Phi(t, t_0)\xi_0 + \int_{t_0}^t \Phi(t, s)u(s)ds$  and kernel  $\tilde{\mathcal{K}}(t, t') = \Phi(t, t_0)\mathcal{K}_0\Phi(t', t_0)^\top + \int_{t_0}^{\min\{t, t'\}} \Phi(t, s)Q_C\Phi(t', s)^\top ds$ ,

**Input:** initial state + task (Maze2D: goal at  $H$ ; KUKA: grasp  $\rightarrow$  place)

$n$ : # of key states,  $d$ : state dimension,  $H$ : planning horizon length

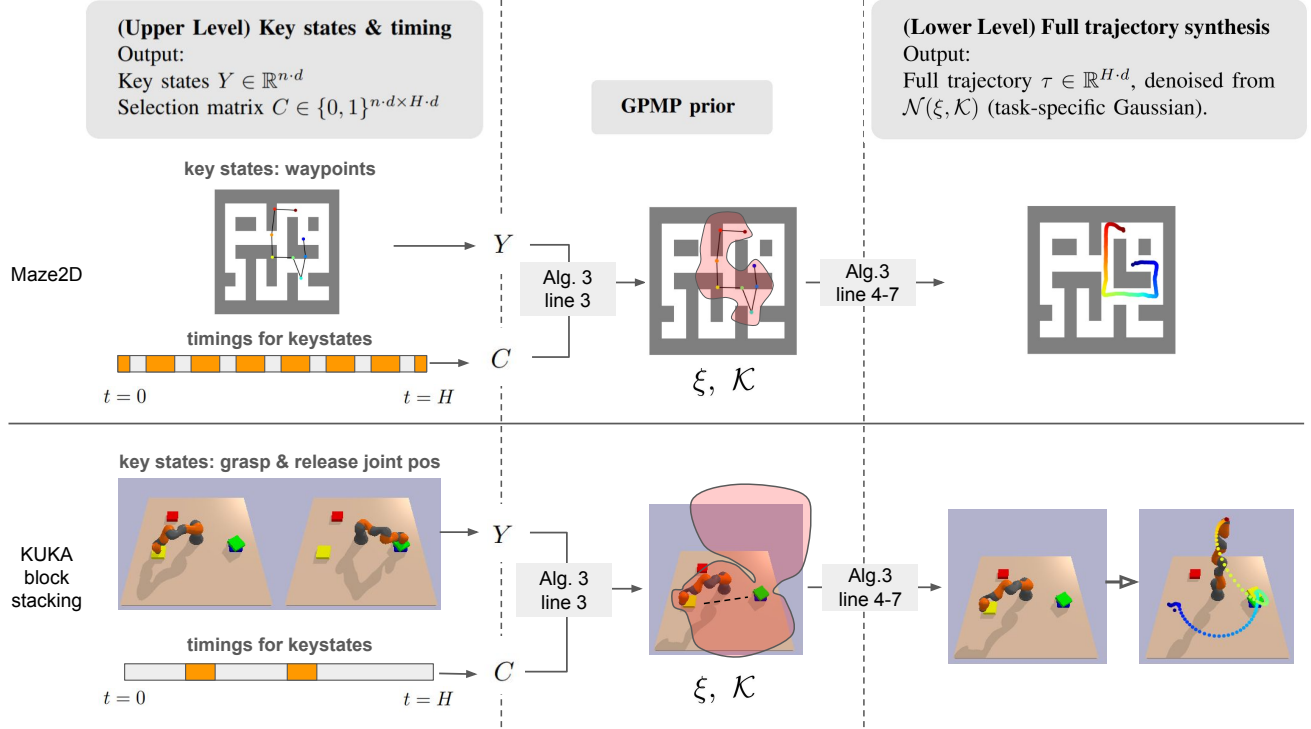


Fig. 1: **Trajectory generation pipeline.** Input: task goal and initial conditions. Upper level produces matrices  $Y$  and  $C$  for sparse key constraint  $C \cdot \tau = Y$ , either by diffusion module and/or rules. (e.g., if the constraints are simple sparse waypoints,  $Y$  is a stack of key states and  $C$  is a selection matrix, which corresponds to designation of timings for the key states.) With  $(Y, C)$ , we construct a Gaussian prior by conditioning a GP over trajectories, yielding  $(\xi, \mathcal{K})$  via (8)–(9). The shaded regions illustrate covariance structure  $\mathcal{K}$  around the trajectory, showing tighter variance near key states and looser variance elsewhere. The lower level then generates the full trajectory by reverse diffusion from  $\mathcal{N}(\xi, \mathcal{K})$ .

which admit sparse and exactly computable discrete counterparts.

Following [1], our work uses a discrete-time version of (4) derived from a constant velocity or constant acceleration model with step  $\Delta t$ . Writing the state at timestep  $t$  as  $x_t$ , the one-step evolution is  $x_{t+1} = \Phi_{t,t+1}x_t + q_t$  with  $q_t \sim \mathcal{N}(0, Q_{t,t+1})$ , where  $\Phi_{t,t+1} = \begin{bmatrix} I & \Delta t I \\ 0 & I \end{bmatrix}$  and  $Q_{t,t+1} = \begin{bmatrix} \frac{1}{3}\Delta t^3 Q_C & \frac{1}{2}\Delta t^2 Q_C \\ \frac{1}{2}\Delta t^2 Q_C & \Delta t Q_C \end{bmatrix}$ . The same structure applies, no matter if the state includes positions only or positions and velocities; velocities can be included explicitly or marginalized to obtain an equivalent GP prior over positions with a block tridiagonal precision matrix. In our experiments, Maze2D uses positions and velocities, whereas the manipulation arm uses joint positions only.

### III. METHOD

Let  $\mathcal{D}$  be a dataset of robot trajectories where each clean sample  $\tau^0 \in \mathcal{D}$  is paired with task information that may admit multiple feasible solutions. It is desirable for the corruption (forward) process to retain task information so that reverse diffusion starts from a task-relevant noise

prior. To this end, we modify the standard DDPM to use a non-isotropic Gaussian with a task conditioned mean and covariance. Reusing the schedule notation from Sec. II-A, with  $\alpha_i = 1 - \beta_i$  and  $\bar{\alpha}_i = \prod_{k=1}^i \alpha_k$ , we define

$$\tau^i \sim \mathcal{N}\left(\sqrt{\alpha_i} \tau^{i-1} + (1 - \sqrt{\alpha_i}) \xi, (1 - \alpha_i) \mathcal{K}\right), \quad (5)$$

where  $\xi \in \mathbb{R}^{H \cdot d}$  and  $\mathcal{K} \in \mathbb{R}^{Hd \times Hd}$  with  $\mathcal{K} \succeq 0$  encode task-dependent trajectory structure.

As in DDPM, (5) yields closed form conditionals with respect to  $\tau^0$ :

$$\tau^i | \tau^0 \sim \mathcal{N}\left(\sqrt{\bar{\alpha}_i} \tau^0 + (1 - \sqrt{\bar{\alpha}_i}) \xi, (1 - \bar{\alpha}_i) \mathcal{K}\right). \quad (6)$$

The one step backward posterior is also Gaussian,

$$q(\tau^{i-1} | \tau^i, \tau^0) = \mathcal{N}(\tau^{i-1}; \tilde{\mu}_i(\tau^i, \tau^0, \xi), \tilde{\beta}_i \mathcal{K}), \quad (7)$$

where

$$\begin{aligned}\tilde{\mu}_i(\tau^i, \tau^0, \xi) &:= \frac{\sqrt{\bar{\alpha}_{i-1}} \beta_i}{1 - \bar{\alpha}_i} \tau^0 + \frac{\sqrt{\alpha_i} (1 - \bar{\alpha}_{i-1})}{1 - \bar{\alpha}_i} \tau^i + \eta_i \xi, \\ \eta_i &:= \frac{1}{1 - \bar{\alpha}_i} [\beta_i (1 - \sqrt{\bar{\alpha}_{i-1}}) - \sqrt{\alpha_i} (1 - \bar{\alpha}_{i-1}) (1 - \sqrt{\alpha_i})], \\ \tilde{\beta}_i &= \left( \frac{\alpha_i}{1 - \alpha_i} + \frac{1}{1 - \bar{\alpha}_{i-1}} \right)^{-1}\end{aligned}$$

are generalization of the DDPM posterior mean and variance coefficient (derivations are given in the Appendix). As  $N \rightarrow \infty$ , the terminal distribution approaches

$$\tau^N \sim \mathcal{N}(\xi, \mathcal{K}).$$

We aim to generate a trajectory  $\tau^0$  that is both smooth and aligned with task constraints. To this end, the mean  $\xi$  and covariance  $\mathcal{K}$  of the non-isotropic Gaussian are constructed using a two-level hierarchy based on GPMP (Sec. II-B). The GP kernel naturally encodes smoothness, while task-specific conditioning is incorporated through GP conditioning, as detailed in Sec. III-B.

The overall planner consists of two components: the upper level produces task-relevant key states and their timings, which are used to construct the task-conditioned prior  $(\xi, \mathcal{K})$ ; the lower level then generates the full trajectory by reverse diffusion under this fixed prior. The inputs are a task specification and an initial condition. The next subsections detail each level.

#### A. Upper level: key states and timings

The upper level identifies task-relevant *key states* and their timings, with simple rule-based heuristics as needed. By key states, we mean boundary conditions, waypoints, or states at contact events.

Given a full trajectory  $\tau \in \mathbb{R}^{Hd}$ , let  $Y = [y_1; \dots; y_n] \in \mathbb{R}^{nd}$  be the stack of  $n$  key states. Define a binary selection matrix  $C \in \{0, 1\}^{nd \times Hd}$  that extracts the key states from the full trajectory, so that  $Y = C \tau$ . Note that the selection matrix  $C$  directly encodes the timings of the key states  $Y$ . The way we construct supervision target for  $(C, Y)$  is task-dependent, and is described in Sec. IV. The complete training process is shown in Alg. 1. We first obtain the ground truth  $(C, Y)$  and choose the supervision targets, which are task dependent. We then update the network parameters of the upper-level diffusion with the standard diffusion loss on the chosen target(s).

#### B. GPMP prior construction

Given the key states  $Y \in \mathbb{R}^{nd}$  and the corresponding selection matrix  $C \in \{0, 1\}^{nd \times Hd}$ , we treat  $Y$  as *soft observations* of the stacked trajectory  $\tau = [x_1; \dots; x_H] \in \mathbb{R}^{H \cdot d}$  with observation covariance  $\mathcal{K}_y \succeq 0$ . The unconditioned GPMP prior (4) induces a GP prior over  $\tau$  with mean  $\tilde{\xi}_- = [\tilde{\xi}_1; \dots; \tilde{\xi}_H] \in \mathbb{R}^{H \cdot d}$  and covariance matrix  $\tilde{\mathcal{K}} = [\tilde{\mathcal{K}}(t_i, t_j)]_{1 \leq i, j \leq H}$ , where subscript  $i$  represents discretized

time step  $i$ . Conditioning this GP prior to the soft observations  $(Y, C, \mathcal{K}_y)$  yields a *task conditioned* posterior over the full trajectory with a closed form mean and covariance [9]

$$\xi = \tilde{\xi} + \tilde{\mathcal{K}} C^\top (C \tilde{\mathcal{K}} C^\top + \mathcal{K}_y)^{-1} (Y - C \tilde{\xi}), \quad (8)$$

$$\mathcal{K} = \tilde{\mathcal{K}} - \tilde{\mathcal{K}} C^\top (C \tilde{\mathcal{K}} C^\top + \mathcal{K}_y)^{-1} C \tilde{\mathcal{K}}. \quad (9)$$

This posterior  $\mathcal{N}(\xi, \mathcal{K})$  serves as the task-conditioned prior for the lower-level reverse diffusion. Small variances in  $\mathcal{K}_y$  enforce tight adherence to key states (e.g., fixed initial or goal states), while larger variances allow flexibility (e.g., soft waypoints). Intuitively,  $Y$  anchors the trajectory near important states and  $\mathcal{K}_y$  encodes confidence in those anchors, without imposing hard constraints.

#### C. Lower level: trajectory generation by denoising

The conditioned prior  $\mathcal{N}(\xi, \mathcal{K})$  determines the non-isotropic and time-correlated Gaussian noise used in our diffusion model; at each step, the injected noise is drawn with a mean and covariance shaped by linear time varying dynamics and the key state and timing information. In particular, the lower level initializes reverse diffusion from  $\mathcal{N}(\xi, \mathcal{K})$  and denoises under the general forward and posterior relations introduced in (6) – (7). For learning, we approximate the reverse posterior (7) with

$$p_\theta(\tau^{i-1} | \tau^i) = \mathcal{N}(\tau^{i-1}; \mu_\theta(\tau^i, i, \text{cond}), \Sigma^i),$$

where *cond* may include  $Y$ ,  $C$ , initial states, and other context, and we take  $\Sigma^i$  to match the scaled structure  $\tilde{\beta}_i \mathcal{K}$ . Following [34] and Sec. II-A, minimizing the KL divergence between  $p_\theta$  and the true reverse posterior reduces to a weighted regression toward  $\tilde{\mu}_i$ . Using the Mahalanobis norm  $\|v\|_A^2 := v^\top A v$ , the training objective becomes

$$L(\theta) = \mathbb{E}_q \left[ \|\tilde{\mu}_i - \mu_\theta(\tau^i, i, \text{cond})\|_{\mathcal{K}^{-1}}^2 \right], \quad (10)$$

up to a scalar schedule dependent factor. This weights errors by the inverse of the task conditioned covariance, encouraging denoising steps that stay consistent with the GP induced temporal coupling and the confidence encoded in  $\mathcal{K}_y$ .

During lower-level training, we use the ground-truth key states and timings  $(C, Y)$ , and perturb them to  $(C + dC_w, Y + dY_w)$  to account for imperfections in the upper-level predictions. The perturbed values are used to instantiate the task-specific prior  $(\xi, \mathcal{K})$  via (8)–(9). We then update the lower-level diffusion parameters using the Mahalanobis MSE loss (10), as summarized in Alg. 2. The complete inference process, including both the upper and lower levels, is summarized in Alg. 3.

*Remark 1:* Computing covariance-related terms  $(C \tilde{\mathcal{K}} C^\top + \mathcal{K}_y)^{-1}$ ,  $\mathcal{K}$ , and  $\mathcal{K}^{-1}$  repeatedly can be costly. We therefore precompute the corresponding gain terms for all timing configurations used at training and inference. For example, in the KUKA manipulation task, we divide the horizon  $H$  into 10 bins and precompute gains for all grasp and release bin pairs  $\binom{10}{2} = 45$ , since only

---

**Algorithm 1** Upper-level training for key-state and timing prediction

---

- 1: **Inputs:** dataset  $\mathcal{D}$  of trajectories  $\tau^0$
  - 2: Initialize upper-level diffusion parameters  $\phi$
  - 3: **while** not converged **do**
  - 4:   Sample trajectory  $\tau^0 \sim \mathcal{D}$
  - 5:   Extract supervision targets  $(C, Y)$  from  $\tau^0 \triangleright C$ : timing indices,  $Y$ : key states
  - 6:   Update  $\phi$  using the standard diffusion loss to predict  $C, Y$ , or both
  - 7: **end while**
- 

**Algorithm 2** Lower-level training (for full trajectory)

---

- 1: **Inputs:** dataset  $\mathcal{D}$ , GP prior  $(\tilde{\xi}, \tilde{\mathcal{K}})$
  - 2: Initialize lower-level diffusion module parameters  $\theta$
  - 3: **while** not converged **do**
  - 4:   Sample  $\tau^0 \sim \mathcal{D}$  and extract  $(C, Y)$  from  $\tau^0$
  - 5:    $(C, Y) \leftarrow (C + dC_\omega, Y + dY_\omega) \triangleright dC_\omega, dY_\omega$  are random perturbations
  - 6:    $(\xi, \mathcal{K}) \leftarrow \text{GP-Post}(\tilde{\xi}, \tilde{\mathcal{K}}, C, Y, \mathcal{K}_y)$  via (8)–(9)
  - 7:   Sample  $i \sim \text{Unif}\{1, \dots, N\}$
  - 8:    $\tau^i \sim \mathcal{N}(\sqrt{\bar{\alpha}_i} \tau^0 + (1 - \sqrt{\bar{\alpha}_i}) \xi, (1 - \bar{\alpha}_i) \mathcal{K})$
  - 9:   Gradient descent  $\nabla_\theta \|\tilde{\mu}_i(\tau^i, \tau^0, \xi) - \mu_\theta(\tau^i, i)\|_{\mathcal{K}^{-1}}^2$
  - 10: **end while**
- 

$C$  changes with timing choices. This preserves time range conditioning while keeping online costs low.

*Remark 2:* Motion Planning Diffusion (MPD) [1] applies a GP as a guidance cost only during reverse sampling, while the forward corruption remains isotropic. We instead parameterize the noise with a GP: conditioning on key states sets the mean  $\xi$  and covariance  $\mathcal{K}$  that govern both the forward and posterior distributions.

## IV. EXPERIMENTS

### A. Experimental Setup

We evaluate the proposed structured-noise formulation on two domains. We describe the benchmark tasks and how task-specific key states and timings are defined.

(i) **Maze2D goal reaching.** Each task specifies a start and a goal state on a fixed maze. In this example, key states are evenly spaced temporal waypoints between the start and the goal, so  $C$  is fixed by design since the waypoint timings—and thus the selection indices—are predetermined. The upper-level diffusion is trained to generate the waypoint set  $Y$  at fixed times  $C$ . These waypoints instantiate the task-conditioned GP prior, from which the lower level generates full trajectories by reverse diffusion.

(ii) **KUKA arm block stacking.** The task is grasp-and-place with a 7-DoF KUKA arm. The dataset provides joint-position trajectories together with a binary contact-flag trajectory (one bit per time step, where 1 indicates contact) for each block; block poses are determined deterministically from kinematics and contact.

---

**Algorithm 3** Test-time Planning (Inference)

---

- 1: **Inputs:** task spec (start/goal, blocks), trained  $\phi$  and  $\theta$ , GP prior  $(\tilde{\xi}, \tilde{\mathcal{K}})$
  - 2: **Upper level:** produce  $(C, Y) \triangleright$  from diffusion model  $\phi$  and rule-based heuristic
  - 3:  $(\xi, \mathcal{K}) \leftarrow \text{GP-Post}(\tilde{\xi}, \tilde{\mathcal{K}}, C, Y, \mathcal{K}_y)$  via (8)–(9)
  - 4: **Lower Level:**
  - 5:  $\tau^N \sim \mathcal{N}(\xi, \mathcal{K})$
  - 6: **for**  $i = N, \dots, 1$  **do**
  - 7:    $\tau^{i-1} \sim \mathcal{N}(\mu_\theta(\tau^i, i), \tilde{\beta}_i \mathcal{K})$
  - 8: **end for**
  - 9: **return**  $\tau^0$
- 

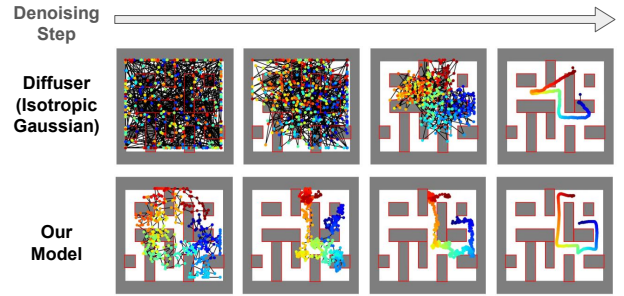


Fig. 2: **Reverse diffusion in Maze2D.** Columns show intermediate denoising steps (left to right). *Top:* isotropic Gaussian prior—samples start fully random and remain noisy until late steps. *Bottom:* our model—initialization is already task-aware and trajectories quickly converge to smooth, goal-reaching solutions.

Key states are defined as the joint configurations at grasp and release events. Accordingly, the upper-level diffusion is trained to predict the contact-flag trajectory, from which grasp and release timings are extracted. Given a ground-truth trajectory  $\tau^0$  and its contact flags, the grasp configuration is defined as the joint state at the first  $0 \rightarrow 1$  transition, and the release configuration as the joint state at the first  $1 \rightarrow 0$  transition. The key-state stack  $Y$  consists of the initial joint state together with these grasp and release configurations, while the selection matrix  $C$  is given by the contact-flag trajectory over the horizon.

At test time, grasp and release block targets are selected using simple heuristics: (1) if a block is currently grasped, it is used as the grasp target; (2) the release target is chosen as the block with the largest vertical position, excluding any grasped block; (3) if no block is grasped, the block closest to the initial end-effector position is selected; (4) if the chosen grasp–release pair is already stacked, a different grasp block is selected. After block target selection, the corresponding grasp and release joint states are computed via inverse kinematics (IK) to form  $Y$ , and the upper-level diffusion predicts the contact-flag trajectory  $C$ .

### B. Baselines and Ablations

We compare three planners in addition to ours that share the same UNet backbone and training schedule, differing

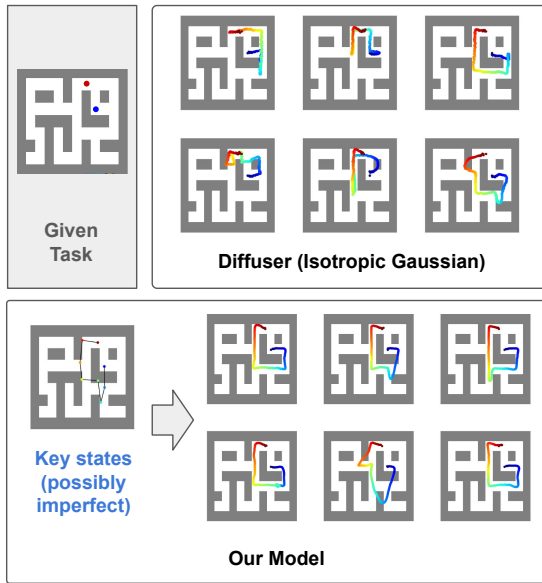


Fig. 3: **Maze2D goal reaching.** Top-Left: task map with start (blue) and goal (red). Top-right: baseline (Diffuser) samples. Bottom: our method. The small inset on the left shows the waypoints predicted by the upper level, which might be imperfect. Thus, instead of hard constraints, we model them as noisy observations.

only in how task structure is incorporated. All models are trained for the same number of optimization steps (100k steps with batch size 32), and we verified that their training losses converged, ensuring that performance differences arise from the choice of noise structure and task representation.

The detailed design of each planner is as follows:

(i) **Diffuser.** The baseline Diffuser [2], which uses isotropic Gaussian noise and conditions only on task inputs such as initial and goal states.

(ii) **Diffuser + KeyCond.** A hierarchical variant of Diffuser where the lower-level diffusion is conditioned on key states and their timings produced by the upper level, while still using isotropic Gaussian noise. This isolates the effect of neural task conditioning without structured noise.

(iii) **EDMP.** A single-level diffuser with isotropic Gaussian noise, guided at inference time by model-based cost functions. Following the general framework of [35], we design task-specific cost functions for each benchmark. For *Maze2D*, the cost penalizes collisions by summing penetration depths of each state with the maze obstacles, together with penetration depths at the midpoints between adjacent states to approximate swept-volume collisions. This implementation requires access to the maze geometry at test time. For *KUKA block stacking*, since [35] does not specify a cost for grasp-and-place tasks, we design a simple heuristic cost based on the minimum distance between the end-effector and target blocks, rewarding configurations with small distance.

(iv) **Hierarchical GPMP (Ours).** Our two-level approach, where the upper level predicts key states and timings, and the lower level denoises under a GPMP-conditioned prior.

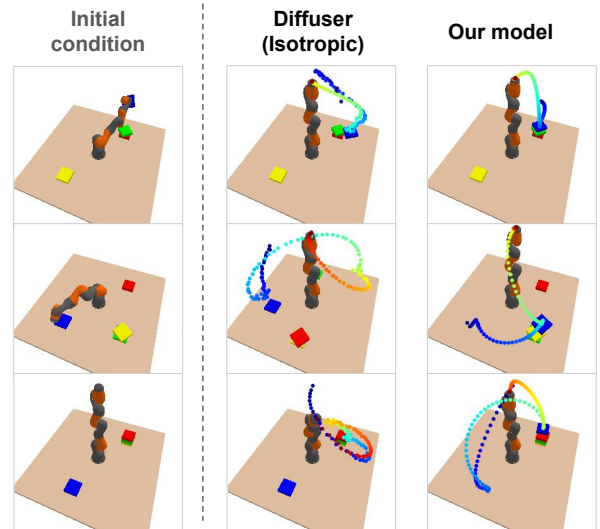


Fig. 4: **Comparison of generated trajectories for KUKA block stacking.** Each row shows a task with a random initial arm configuration and block positions. Columns: (left) initial condition, (middle) trajectories generated with an isotropic Gaussian prior, (right) trajectories generated with our model.

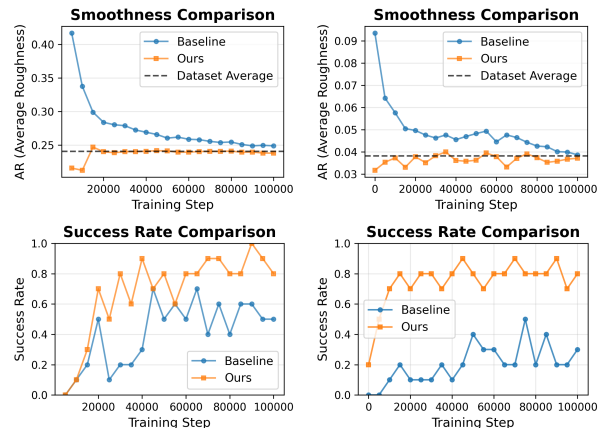


Fig. 5: Average roughness (AR) and success rate over training for *Maze2D* (left) and *KUKA* (right). Metric calculated as average of 10 samples. The dashed line shows the dataset-average AR as a reference for reasonable smoothness.

Note that the choice of noise prior applies only to the lower-level diffusion. Whenever a hierarchical model is used, the upper-level diffusion always employs a standard DDPM with isotropic Gaussian noise.

### C. Results and Analysis

**Task encoding with GPMP conditioning enables high success rates.** In *Maze2D*, a trajectory is considered successful if (i) the final state lies within a predefined tolerance radius of the goal and (ii) the trajectory remains collision-free with respect to the maze map. Results are averaged over 100 randomly sampled start–goal pairs. In *KUKA block stacking*, success requires both a valid grasp and placement within tolerance. A grasp is successful if the end-effector is within a spatial threshold of the target block at the first contact onset

Method	Maze2D	KUKA Stacking
Diffuser	48/100	31/100
Diffuser + KeyCond	49/100	28/100
EDMP	56/100	34/100
Hierarchical GPMP (Ours)	<b>81/100</b>	<b>70/100</b>

TABLE I: Task success rates over 100 samples.

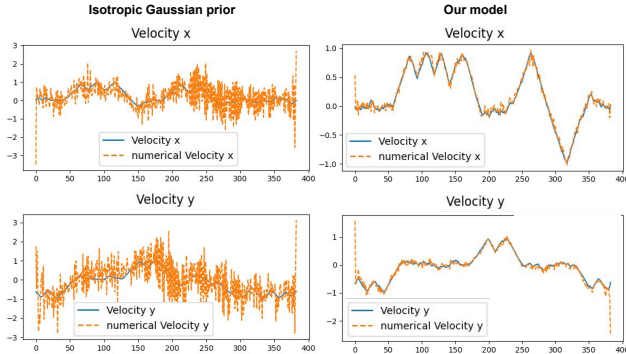


Fig. 6: **Maze2D velocity consistency.** Left: isotropic Gaussian prior; Right: our model. Blue: generated velocities; Orange: numerical derivatives of generated positions. Closer alignment indicates better dynamic feasibility.

(flag transition  $0 \rightarrow 1$ ). Placement is successful if, at release time, the end-effector lies within tolerance of the designated stacking location. Results are averaged over 100 randomized initial joint configurations and block layouts.

Table I shows that our method achieves the best success rates across both tasks. This improvement can be attributed to the structured prior, which concentrates probability mass near task-critical trajectories through soft conditioning in (8)–(9).

The results of *Diffuser + KeyCond* further indicate that the primary benefit arises from the structured noise model rather than from neural conditioning alone. We encode  $(Y, C)$  with a lightweight MLP and use the resulting features to condition the diffusion model for both *Diffuser + KeyCond* and our method, enabling a controlled comparison that isolates the effect of the noise structure.

**LTV-GP-based covariance produces smoother trajectories.** We evaluate the smoothness of the generated trajectories using both qualitative and quantitative measures. For quantitative evaluation, we adopt the *Average Roughness* (AR) metric [35], defined as the average of  $\|x_{t+1} - x_t\|$  along the trajectory. Lower AR corresponds to smoother trajectories; however, excessively low values (e.g.,  $AR = 0$ , corresponding to no movement) are not desirable. We therefore compare the AR of generated trajectories against the ground-truth AR computed from the dataset. (See Fig. 5). We additionally present representative trajectories (Fig. 3, Fig. 4) and their denoising processes (Fig. 2) for qualitative comparison.

**LTV-GP covariance captures inter-state dependencies.** We evaluate whether generated trajectories preserve dependencies between state dimensions. In the Maze2D benchmark, the Diffuser baseline outputs position, velocity, and action-effort sequences. Our method instead employs a GPMP-inspired prior that explicitly couples position and

Maze2D (100 samples)	Velocity MAE
Diffuser	0.2187
Diffuser + KeyCond	0.2064
EDMP	0.2012
Hierarchical GPMP (Ours)	<b>0.0767</b>

TABLE II: Maze2D velocity consistency: mean absolute error (MAE) between generated velocities and finite-difference derivatives of positions over 100 trajectories.

velocity through the LTV-GP covariance, encouraging dynamically feasible trajectories. To assess this property, we compare predicted velocities with finite-difference derivatives of positions (Fig. 6) and report the mean absolute error (MAE) over the trajectory horizon (Table II).

Overall, our method produces trajectories with stronger position–velocity consistency, whereas the baseline often exhibits jagged position traces and inconsistent velocity profiles—especially near hard start and goal constraints—leading to dynamically infeasible behavior.

**Encoding task information in the prior improves training efficiency.** The structured prior preserves task-related information during the corruption process, leading to more efficient training. We report average roughness (AR) and success rate (SR) over training steps in Fig. 5. While the vanilla Diffuser gradually produces smoother trajectories as training progresses, our method achieves dataset-level smoothness from early stages due to the structured prior, whereas the baseline requires substantially more training to reach comparable AR values.

A similar trend is observed for SR: our method attains high SR at early training stages. Notably, desirable trajectory properties such as smoothness and task success do not necessarily converge with the diffusion training loss. Thus, relying on training loss alone makes it difficult to identify a desirable operating point. Although longer training may eventually improve these metrics, diffusion models are computationally expensive, making such prolonged training inefficient.

**Separating timing prediction enables modeling phase-dependent task structure.** In many robotics tasks, desired behavior depends not only on the time index but also on the task phase (e.g., grasp, transport, and release in the KUKA example). Encoding such phase-dependent behavior through cost guidance is challenging. While collision-avoidance costs can evaluate each state independently (e.g., checking whether a state is in collision), tasks that require interactions at precise moments create strong coupling between timing variables (e.g., the contact-flag trajectory) and robot joint states. Moreover, cost-guided diffusion must evaluate partially denoised trajectories during sampling, where interaction times can shift significantly under noise. These factors make such non-stationary task structures difficult to represent with a differentiable cost.

Our framework addresses this by assigning timing prediction to the upper level while the lower level generates trajectories conditioned on these predictions with uncertainty. This separation enables more effective modeling of phase-

dependent behaviors and contributes to the improved performance in Table I.

## V. CONCLUSION

In this paper, we propose a hierarchical diffusion planner that embeds task and motion structure directly in the noise model. We validate the approach through experiments on two robotic domains, where our method demonstrates improved task success and trajectory quality, such as smoother trajectories and better inter-state coupling consistency.

Although we use a lightweight diffusion model at the upper level, the lower level is agnostic to *how* the key states are obtained—be it rule-based, model-based, or learned. Moreover, our method does not require handcrafted reward terms or auxiliary objectives for guidance, and it does not rely on advanced neural architectures beyond conditioning on upper-level-generated features.

Future work includes applying the framework to more complex robotic systems (e.g., humanoids) and incorporating more advanced task specifiers, such as VLM-based modules, at the upper level.

## REFERENCES

- [1] J. Carvalho, A. T. Le, M. Baierl, D. Koert, and J. Peters, “Motion planning diffusion: Learning and planning of robot motions with diffusion models,” in *2023 IEEE/RSJ International Conference on Intelligent Robots and Systems (IROS)*. IEEE, 2023, pp. 1916–1923.
- [2] M. Janner, Y. Du, J. Tenenbaum, and S. Levine, “Planning with diffusion for flexible behavior synthesis,” in *International Conference on Machine Learning*. PMLR, 2022, pp. 9902–9915.
- [3] C. Chi, Z. Xu, S. Feng, E. Cousineau, Y. Du, B. Burchfiel, R. Tedrake, and S. Song, “Diffusion policy: Visuomotor policy learning via action diffusion,” *The International Journal of Robotics Research*, p. 02783649241273668, 2023.
- [4] A. Ajay, Y. Du, A. Gupta, J. Tenenbaum, T. Jaakkola, and P. Agrawal, “Is conditional generative modeling all you need for decision-making?”
- [5] R. P. Wolf, Y. Shi, S. Liu, and R. Rayyes, “Diffusion models for robotic manipulation: A survey,” *Frontiers in Robotics and AI*, vol. 12, p. 1606247, 2025.
- [6] S. Yan, Z. Zhang, M. Han, Z. Wang, Q. Xie, Z. Li, Z. Li, H. Liu, X. Wang, and S.-C. Zhu, “M 2 diffuser: Diffusion-based trajectory optimization for mobile manipulation in 3d scenes,” *IEEE Transactions on Pattern Analysis and Machine Intelligence*, 2025.
- [7] K. Mizuta and K. Leung, “Cobl-diffusion: Diffusion-based conditional robot planning in dynamic environments using control barrier and lyapunov functions,” in *2024 IEEE/RSJ International Conference on Intelligent Robots and Systems (IROS)*. IEEE, 2024, pp. 13 801–13 808.
- [8] C. Pan, Z. Yi, G. Shi, and G. Qu, “Model-based diffusion for trajectory optimization,” *Advances in Neural Information Processing Systems*, vol. 37, pp. 57 914–57 943, 2024.
- [9] M. Mukadam, J. Dong, X. Yan, F. Dellaert, and B. Boots, “Continuous-time gaussian process motion planning via probabilistic inference,” *The International Journal of Robotics Research*, vol. 37, no. 11, pp. 1319–1340, 2018.
- [10] M. Seo, Y. Cho, Y. Sung, P. Stone, Y. Zhu, and B. Kim, “Presto: Fast motion planning using diffusion models based on key-configuration environment representation,” in *2025 IEEE International Conference on Robotics and Automation (ICRA)*. IEEE, 2025, pp. 10 861–10 867.
- [11] W. Xiao, T.-H. Wang, C. Gan, R. Hasani, M. Lechner, and D. Rus, “Safediffuser: Safe planning with diffusion probabilistic models,” in *The Thirteenth International Conference on Learning Representations*, 2023.
- [12] C.-C. Hsu, B. Wen, J. Xu, Y. Narang, X. Wang, Y. Zhu, J. Biswas, and S. Birchfield, “Spot: Se(3) pose trajectory diffusion for object-centric manipulation,” in *2025 IEEE International Conference on Robotics and Automation (ICRA)*. IEEE, 2025, pp. 4853–4860.
- [13] J. Urain, N. Funk, J. Peters, and G. Chalvatzaki, “Se (3)-diffusionfields: Learning smooth cost functions for joint grasp and motion optimization through diffusion,” pp. 5923–5930, 2023.
- [14] J.-B. Bouvier, K. Ryu, K. Nagpal, Q. Liao, K. Sreenath, and N. Mehr, “Ddat: Diffusion policies enforcing dynamically admissible robot trajectories,” *arXiv preprint arXiv:2502.15043*, 2025.
- [15] J. Liang, J. K. Christopher, S. Koenig, and F. Fioretto, “Simultaneous multi-robot motion planning with projected diffusion models,” pp. 37 162–37 180, 2025.
- [16] Z. Yin, T. Lai, L. Barcelos, J. Jacob, Y. Li, and F. Ramos, “Diverse motion planning with stein diffusion trajectory inference,” in *2025 IEEE International Conference on Robotics and Automation (ICRA)*. IEEE, 2025, pp. 15 610–15 616.
- [17] R. Wu, H. Chen, M. Zhang, H. Lu, Y. Li, and Y. Li, “Neural dynamics augmented diffusion policy,” in *2025 IEEE International Conference on Robotics and Automation (ICRA)*. IEEE, 2025, pp. 13 234–13 241.
- [18] E. Nachmani, R. S. Roman, and L. Wolf, “Non gaussian denoising diffusion models,” *arXiv preprint arXiv:2106.07582*, 2021.
- [19] X. Yu, X. Gu, H. Liu, and J. Sun, “Constructing non-isotropic gaussian diffusion model using isotropic gaussian diffusion model for image editing,” *Advances in Neural Information Processing Systems*, vol. 36, pp. 76 839–76 851, 2023.
- [20] C. Curreli, D. Muhle, A. Saroha, Z. Ye, R. Marin, and D. Cremers, “Nonisotropic gaussian diffusion for realistic 3d human motion prediction,” pp. 1871–1882, 2025.
- [21] N. Jia, T. Zhu, H. Liu, and Z. Zheng, “Structured diffusion models with mixture of gaussians as prior distribution,” *arXiv preprint arXiv:2410.19149*, 2024.
- [22] L. Wang, H. Yu, C. Yu, S. Gao, and H. Christensen, “Controllable motion generation via diffusion modal coupling,” *arXiv preprint arXiv:2503.02353*, 2025.
- [23] D. Blessing, X. Jia, and G. Neumann, “End-to-end learning of gaussian mixture priors for diffusion sampler.”
- [24] H. Guo, C. Lu, F. Bao, T. Pang, S. Yan, C. Du, and C. Li, “Gaussian mixture solvers for diffusion models,” *Advances in Neural Information Processing Systems*, vol. 36, pp. 25 598–25 626, 2023.
- [25] X. Zhou, X. Chen, and J. Yang, “Diff-refiner: Enhancing multi-agent trajectory prediction with a plug-and-play diffusion refiner,” in *2025 IEEE International Conference on Robotics and Automation (ICRA)*. IEEE, 2025, pp. 10 779–10 785.
- [26] J. E. Liang, “Diffusion models for robotics,” in *Proceedings of the AAAI Conference on Artificial Intelligence*, vol. 39, no. 28, 2025, pp. 29 587–29 589.
- [27] H. Ren, Y. Zeng, Z. Bi, Z. Wan, J. Huang, and H. Cheng, “Prior does matter: Visual navigation via denoising diffusion bridge models,” in *Proceedings of the Computer Vision and Pattern Recognition Conference*, 2025, pp. 12 100–12 110.
- [28] C. Chen, F. Deng, K. Kawaguchi, C. Gulcehre, and S. Ahn, “Simple hierarchical planning with diffusion,” 2024.
- [29] M. Sharma, A. Fishman, V. Kumar, C. Paxton, and O. Kroemer, “Cascaded diffusion models for neural motion planning,” pp. 14 361–14 368, 2025.
- [30] Z. Dong, J. Hao, Y. Yuan, F. Ni, Y. Wang, P. Li, and Y. Zheng, “Diffuserlite: Towards real-time diffusion planning,” *Advances in Neural Information Processing Systems*, vol. 37, pp. 122 556–122 583, 2024.
- [31] D. Wang, C. Liu, F. Chang, and Y. Xu, “Hierarchical diffusion policy: manipulation trajectory generation via contact guidance,” *IEEE Transactions on Robotics*, 2025.
- [32] X. Ma, S. Patidar, I. Haughton, and S. James, “Hierarchical diffusion policy for kinematics-aware multi-task robotic manipulation,” in *Proceedings of the IEEE/CVF Conference on Computer Vision and Pattern Recognition*, 2024, pp. 18 081–18 090.
- [33] G. Nandiraju, Y. Ju, C. Xu, and H. Wang, “Hdflow: Hierarchical diffusion-flow planning for long-horizon robotic assembly,” in *NeurIPS 2025 Workshop on Embodied World Models for Decision Making*, 2025.
- [34] J. Ho, A. Jain, and P. Abbeel, “Denoising diffusion probabilistic models,” *Advances in neural information processing systems*, vol. 33, pp. 6840–6851, 2020.
- [35] K. Saha, V. Mandadi, J. Reddy, A. Srikanth, A. Agarwal, B. Sen, A. Singh, and M. Krishna, “Edmp: Ensemble-of-costs-guided diffusion for motion planning,” in *2024 IEEE International Conference on Robotics and Automation (ICRA)*. IEEE, 2024, pp. 10 351–10 358.

APPENDIX

A. *Derivation of Marginal  $q(\tau^j | \tau^0)$  in (6)*

We proceed by induction. Assume (6) holds for  $i = j - 1$ . Then,  $\tau^j | \tau^0$  is Gaussian with mean and variance

$$\begin{aligned}\mathbb{E}[\tau^j | \tau^0] &= \sqrt{\alpha_j} \mathbb{E}[\tau^{j-1} | \tau^0] + (1 - \sqrt{\alpha_j})\mu \\ &= \sqrt{\alpha_j} (\sqrt{\bar{\alpha}_{j-1}}\tau^0 + (1 - \sqrt{\bar{\alpha}_{j-1}})\mu) + (1 - \sqrt{\alpha_j})\mu \\ &= \sqrt{\bar{\alpha}_j} \tau^0 + (1 - \sqrt{\bar{\alpha}_j})\mu, \\ \text{Var}[\tau^j | \tau^0] &= \alpha_j(1 - \bar{\alpha}_{j-1})\mathcal{K} + (1 - \alpha_j)\mathcal{K} = (1 - \bar{\alpha}_j)\mathcal{K}.\end{aligned}$$

Hence the form holds for step  $j$ , as claimed.

B. *Derivation of Posterior (7)*

The posterior is obtained using Bayes' rule:

$$q(\tau^{i-1} | \tau^i, \tau^0) \propto q(\tau^i | \tau^{i-1}) q(\tau^{i-1} | \tau^0).$$

Both  $q(\tau^i | \tau^{i-1})$  and  $q(\tau^{i-1} | \tau^0)$  are Gaussian distributions with known forms given in (5)–(6). Combining these expressions yields the Gaussian posterior in (7).